Design of a Manufacturing Demonstration Unit for a Composite Lunar Landing Gear Strut

Brian H. Mason,[1]
NASA Langley Research Center, Hampton, VA 23681-2199

Alana Zahn,[2] Kevin E. Gould[3], and
Analytical Mechanics Associates, Inc., Hampton, VA 23666

Adam Przekop[4]
NASA Langley Research Center, Hampton, VA 23681-2199

The goal of the current work was to develop an analytical framework for design of composite struts using various levels of model fidelity. Rapid optimization trade studies were performed using low fidelity two-dimensional (2D) axisymmetric models with smeared composite properties. The optimum 2D model was compared with three-dimensional (3D) models with higher levels of fidelity in material property representation. Good agreement was found with all models. The buckling performance of the highest fidelity 3D model was found to be satisfactory for the intended loading conditions. An additional goal of this work was to perform an initial assessment of using automated fiber placement (AFP) and other advanced manufacturing methods to explore their feasibility for the fabrication of struts for lunar landers, strut-braced wings, and other aerospace components. The designs produced during this study are intended to be used to develop manufacturing demonstration units (MDU) that can be fabricated at the Integrated Structural Assembly of Advanced Composites (ISAAC) facility at Langley Research Center (LaRC) and tested in lab facilities at LaRC.

I. Introduction

A mission of NASA is the design and evaluation of future aircraft and spacecraft concepts. Part of this mission involves evaluating the efficiency of structural concepts for aircraft and spacecraft components with the goal of designing lightweight parts. Currently, NASA researchers are interested in structurally efficient truss structures for application to spacecraft and aircraft components such as solar array supports, lunar lander struts, strut-braced wing components, and aircraft spars for unmanned aerial vehicles.

Structural efficiency herein is defined as the ratio of the load-carrying ability to the mass of a structure. Studies involving the structural efficiency of shells have been ongoing at NASA for decades and continue today [1 to 7]. Composite materials and nontraditional designs offer opportunities for reduced mass compared to conventional aluminum trusses with uniform circular cross-sections. An example of a structure that would have been dependent upon struts in a truss arrangement is the Altair lunar lander [8] as shown in Fig. 1. Composite struts were evaluated for use with the Altair lander [9 to 17], and structurally efficient truss members such as composite struts are still of interest to NASA for space applications. The work discussed in this paper is an expansion of the strut research from the previous Altair lander work.

[1] Research Aerospace Engineer, Structural Mechanics and Concepts Branch, Mail Stop 190, AIAA Associate Fellow.
[2] Aerospace Engineer, Analytical Mechanics Associates, Resident at NASA LaRC, Mail Stop 190, AIAA Student Member.
[3] Structural Engineering Analyst, Analytical Mechanics Associates, Resident at NASA LaRC, Mail Stop 190.
[4] Research Aerospace Engineer, Structural Mechanics and Concepts Branch, Mail Stop 190, AIAA Associate Fellow.

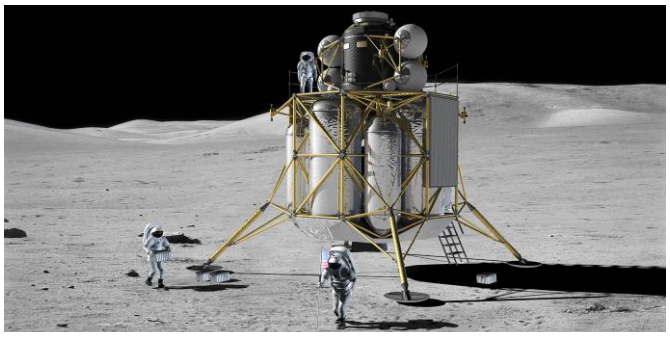

Fig. 1. Altair lunar lander.

The goal of the current work was to develop an analytical framework for design of composite struts using various levels of model fidelity. An additional goal of this work was to perform an initial assessment of using automated fiber placement (AFP) and to explore its feasibility for the fabrication of struts for lunar landers, strut-braced wings, and other aerospace components. In particular, designs were considered for fabrication at the Integrated Structural Assembly of Advanced Composites (ISAAC) facility at Langley Research Center (LaRC), shown in Fig. 2. The designs produced during this study are intended to be used to develop manufacturing demonstration units (MDU) that can be fabricated at ISAAC and tested in lab facilities at LaRC.

Fig. 2. ISAAC manufacturing robot.

This paper is organized as follows. In Section II, development of the geometry and material properties from legacy documentation is discussed. Development of a parametric finite element (FE) model is discussed in Section III. Next, in Section IV, the optimization framework used to size the cross-sectional geometry of the MDU strut is described. In Section V, analytical results from a two-dimensional (2D) axisymmetric FE model and three three-dimensional (3D) solid element models of the optimized MDU design are presented. Results of the study are summarized in Section VI.

II. Geometry and Material Properties of Landing Gear Strut

The landing gear assembly for the Altair lander consisted of multiple struts and fittings with different geometries and loading conditions. As a demonstration unit for manufacturing composite struts at ISAAC, a strut designed, built, and tested from work conducted by Northrop Grumman Corporation [13 and 15] was selected as a starting point for the unit discussed in this paper. In this section the reference strut [15] is discussed first, followed by a discussion of the changes made to create the current design.

The Northrop-Grumman-designed strut assembly consisted of a composite tubular body and two metallic fitting regions, as shown in Fig. 3. The composite body was a single-piece tubular laminate with tapered ends that attach to an end fitting region, as shown in Fig. 4a. Composite overwraps for increased hoop strength were added in the fitting region. The metallic inserts in the fitting region of the strut were made of 6Al-4V titanium alloy and consisted of an

integral corrugated insert. The tube laminate was IM7-8552 carbon fiber/epoxy with a ply thickness of 0.0052 in. and a stacking sequence of $[90/0_2/\pm45/0_3/90]_s$ [15]. The overwraps were 90° plies of the same carbon fiber/epoxy. Elastic properties for the titanium and carbon fiber/epoxy are given in Table 1.

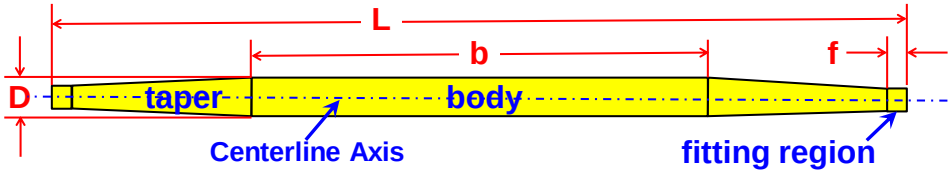

Fig. 3. Geometry of a typical landing gear strut.

Table 1. Assumed material properties

Property	IM7-8552 [15]	Toray T800 [18]	Titanium [15]
Elastic Modulus – Longitudinal, Msi	21.40	20.25	16.00
Elastic Modulus – Transverse, Msi	1.46	1.20	16.00
Shear Modulus, Msi	0.69	0.57	6.06
Poisson's Ratio	0.30	0.33	0.32

A cross-sectional view of the fitting region of the reference strut [15] is shown in Fig. 4a, where tube refers to the tube laminate that is sandwiched between the overwrap and the metallic insert. The station numbers, shown in Fig. 4, refer to the locations of peaks or valleys in the insert region geometry. The metallic insert was corrugated in order to create a mechanical-locking effect in the primary load path of the composite strut. In the reference work, the composite was wrapped around the metallic inserts using a mandrel and hand-layup. The strut design in this paper differs from the reference design in several areas, which are discussed in the following paragraphs.

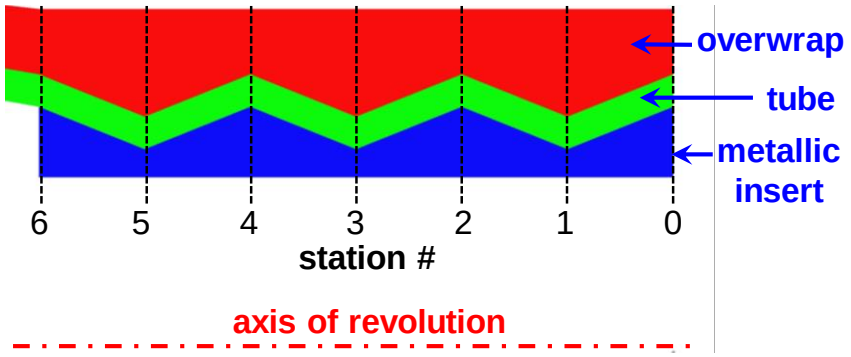

(a) Cross section of legacy fitting region [15]

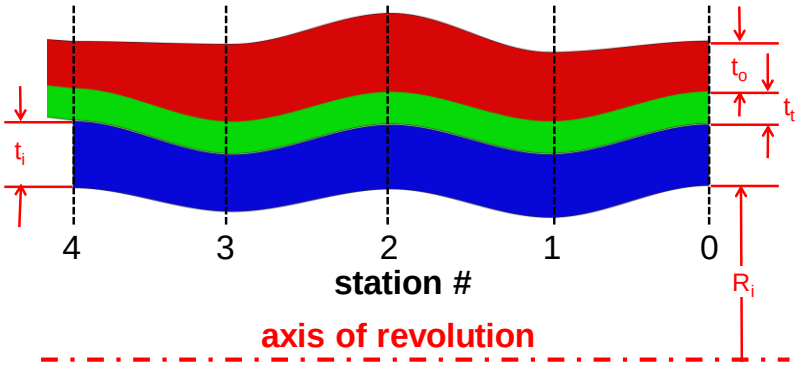

(b) Cross section of fitting region improved for manufacturing

Fig. 4. Geometry of a typical landing gear strut.

For the work discussed in this paper, AFP was desired to build the MDU composite strut, but the sharp corners of the insert made AFP in the fitting region difficult. As an alternative design, the fitting shown in Fig. 4b was developed with sinusoidal corrugation profiles that were much easier for the compaction rollers on the AFP head to traverse, rather than the sharp corners within the original design. All design trials in this paper were performed with the sinusoidal fitting shown in Fig. 4b with two humps instead of three for improved manufacturability.

Initial guidance for the dimensions of the MDU strut design was available from the reference strut [15] as shown in Table 2, but some alterations were made based on available material and new geometry requirements. Specifically, the tube laminate composite was changed from IM7-8552 to Toray T800S-3900-25K [18] with a stacking sequence of $[\pm 45/0/45/90/-45/0_2/45/90/-45/0]_s$ and a nominal ply thickness of 0.0039 in. Also, the strut length for the new design is different from the Altair [15] design, as given in Table 2. As shown in a trial of AFP placement with ISAAC in Fig 5, steep taper angles resulted in significant wrinkling and gaps during tow placement. To reduce the taper angle from the reference design, the taper length was increased to 22 in., which corresponded to a body length of 55.114 in. when preserving the total strut length. Additional trials are planned with ISAAC to evaluate the effect of these geometric changes on the AFP process. A summary of the overall strut dimensions is provided in Table 2.

Specific cross-sectional dimensions for the fitting were not provided in Fig. 4, because they were developed in the design process discussed in Section IV below. Reference dimensions [15] were used to find the range of values for the inner radius and thicknesses of the fitting as shown in Table 3; although, the inner radius of the metallic insert was allowed to vary instead of being kept constant. Different variables from Fig. 4b are used to define the inner radius, insert thickness, and overwrap thickness at each of the five axial station locations. The main tube thickness is assumed to be identical at all five stations even though small thickness variations are introduced by placing the same amount of composite material over a slightly varying circumference of the insert. The laminate stacking sequence of the tube was kept the same, but the ply thicknesses were varied with the intent of using standard and thin plies in the final manufactured part to produce a laminate with a stiffness similar to the one selected by the optimization process. The dimensions of the MDU were then iterated using these variables as discussed in the following sections.

Fig. 5. Layup issues in ISAAC AFP trial article.

Table 2. Dimensions of a typical landing gear strut.

Dimension	Initial Values [15], in.	Adjusted Values, in.
Strut Length (L)	77.660	105.000
Body Length (b)	50.670	55.114
Fitting Length (f)	2.943	2.943
Inner Diameter of Body (D)	6.000	4.750

Table 3. Cross sectional dimensions of fitting region in strut.

Dimension	Minimum, in.	Maximum, in.
Inner Radius (R_i)	0.60	1.30
Insert Thickness (t_i)	0.10	0.50
Tube Thickness (t_t)	0.0672	0.1008
Overwrap Thickness (t_o)	0.10	0.35

III. Parametric Finite Element Model

A parametric FE model of the landing gear was generated from the geometry presented in Section II. Analyses were performed using the general-purpose FE code Abaqus [19]. The FE model consisted of 4362 CAX4 axisymmetric solid elements and 5413 nodes, and is illustrated in Fig. 6. An axisymmetric modeling approach was used to simplify the modeling effort and analysis time for the optimization scheme described in Section IV. Because layered composites properties cannot be used with the CAX4 elements, laminate properties were represented with smeared properties according to composite lamination theory (CLT). The Abaqus contact surface algorithm was used to define the interaction between the metallic insert (shown in blue) and the composite tube (shown in green). Boundary conditions on the model were applied at the middle of the strut as an axis of symmetry for this half-model, as shown in Fig. 6b.

For design purposes, only a nonlinear static analysis was performed with this model. Loading was applied to the insert as a displacement in the axial direction, as shown in Fig 6b. The lower limit on the reaction force for this applied displacement field was a 27-kip compression load with a 1.5 factor of safety for a total of 40.5 kip.

The design problem was formulated as minimizing the mass of the strut subject to strain limits on the composite section, stress limits in the metallic insert, a constraint to balance the load between the ramp locations, and a lower limit on the reaction force. A design strain limit of 5000 micro strain was selected for all composite regions in the hoop direction. In the axial direction, the 5000 micro-strain design strain limit was applied only to the tube laminate at the center of the strut and fitting regions, and not to the overwrap or transition zones. Because axial strain in the overwraps was not constrained, matrix failure in those zones is possible, but it is not a concern for the strut design. A von Mises yield strength limit of 125 ksi was applied to the metallic insert as a constraint. In the Altair investigation [15], the strain contours at final failure showed significantly nonuniform load distribution within the insert region. The value on the first metallic ramp on the outer edge of the strut was equivalent to about 65% of the load distribution, the middle ramp had about 25%, and the inner-most ramp, closest to the taper, had the remaining roughly 10% of the load distribution. For the MDU, an optimized design was created to level the amount of load each insert ramp transfers. The number of ramps was also decreased from three triangular shapes to two sinusoidal shapes in order to create more gradual strain contours, and also to enable easier manufacture with ISAAC. As an approximation, the measure of balancing the load was a comparison of the overwrap hoop strains in two specific finite elements at select locations on different ramps, shown as ramp #1 and #2 in Fig. 6b. Plots of the stress and strain fields for the optimized design of the MDU strut are presented in Section V.

(a) Full FE model of strut

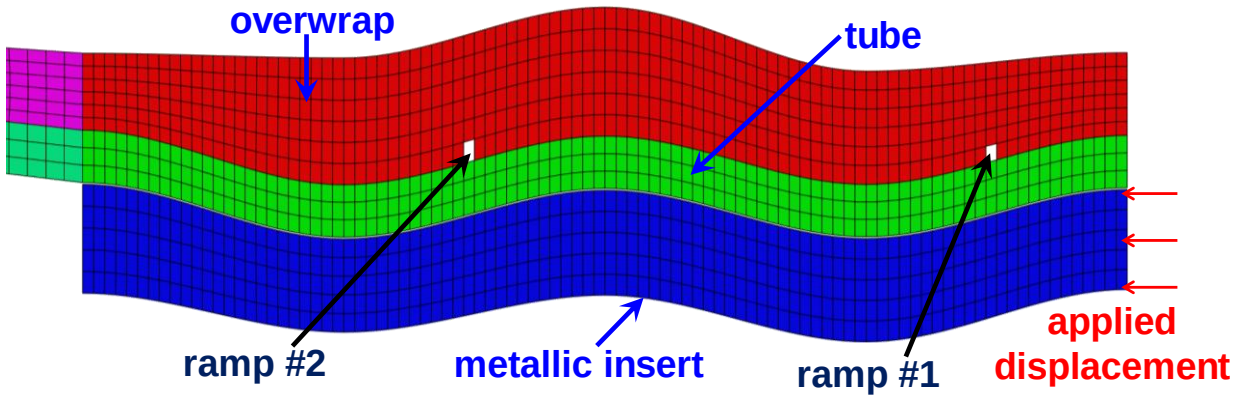

(b) Detail of fixture region in FE model

Fig. 6. Axisymmetric finite element model of strut.

IV. Optimization Framework

An important objective of the present activity is to develop a robust process for tailoring a composite strut design that is lightweight and able to survive operational loads. To accomplish this objective, an optimization framework has been developed using the general-purpose optimization software LS-OPT [20]. The software can be set up to run any command-line driven analysis code, such as a Python script or a FE analysis code. The design study was performed within LS-OPT following the flowchart shown in Fig. 7.

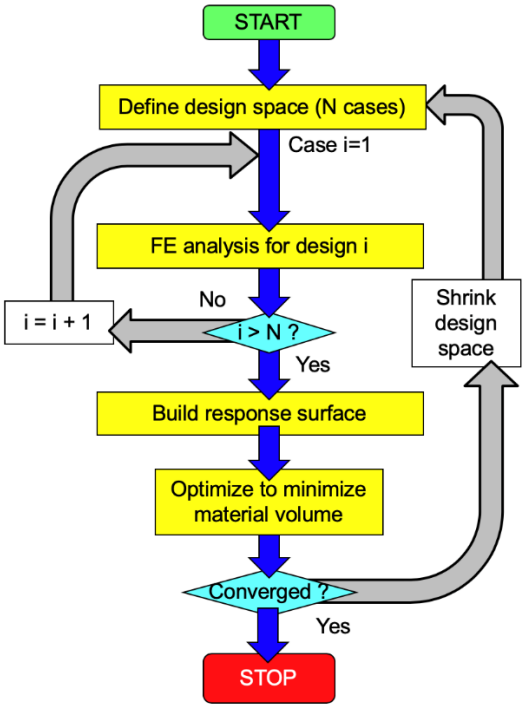

Fig. 7. LS-OPT framework for optimization with FE analysis.

The LS-OPT software performed optimization on a response surface representing the constraints and objective function of the design variables. A Latin Hypercube criterion [21] was used in the framework shown in Fig. 7 to define a design space with 40 sets of design variables (selected from the ranges given in Table 3). LS-OPT then automatically partitioned FE analyses at each of these 40 designations. The stress and strain results from these 40 cases were used to construct a Kriging response surface as an interpolation technique [22].

A script written in the PATRAN Command Language (PCL) [23] was developed to generate the geometry and FE mesh. Additional Python scripts were developed to post-process the results from the Abaqus output database and to parse the data into text files that could be interpreted by the LS-OPT software. Weight was then used as the objective function to be minimized. Because the FE model was axisymmetric, an additional PCL script was developed to revolve the geometry defining the mesh into solids from which the volume of the material in the strut was computed to determine the total weight.

The initial design space was defined using the design variables outlined in Table 3. Two design constraints, the inner radius and the insert thickness, were used to define the shape of the outer surface of the insert. Additionally, the outer radius of the insert at stations 0, 2, and 4 was set to a value of 1.375 in. The outer radius of the insert at stations 1 and 3 was set to a value of 1.15 in. By setting the outer radii of the inserts, the five design variables defining the inner radii became dependent variables with values equal to the outer radii minus the thicknesses of the inserts at those stations. The total number of design variables was eleven (five insert and overwrap thicknesses and one tube thickness).

Three additional constraints were imposed on the design. A maximum axial strain value of 5000 μ strain was imposed on the composite regions in the hoop and axial directions, as described in Section III. Because the load was applied as a displacement, the target compressive load of 40.5 kips was set as a constraint. Finally, the hoop strains at the two ramp locations were constrained to be within 10% of their average values in order to balance the load distribution as discussed in Section III. Sample results from this design study are presented in the next section.

V. Finite Element Analysis Results

The final optimized design of the fitting region has been developed and is shown in Fig 8, and the variable values are given in Table 4. Note that the tube thickness specified in Table 4 is in the middle of the strut. During the manufacturing process, the tube thickness increases in the taper region in order to keep the material volume constant. The actual thickness of the tube in the fixture region is multiplied by the ratio of the tube inner diameter in the middle divided by the diameter of the fixture, resulting in a tube thickness of 0.1617 in. in the fixture. The primary constraint driving this design was the balance of the load between the ramps. Balancing the load was accomplished by setting a limit on the hoop strain values in ramps #1 and #2 as shown in Table 5. The hoop strains in the ramp were within 10% of their average value. In this design, the metallic fitting tapers in thickness from the load application end to the center of the strut, while the overwrap tapers in the opposite direction. To further validate the results of the axisymmetric model, a higher fidelity FE model was created.

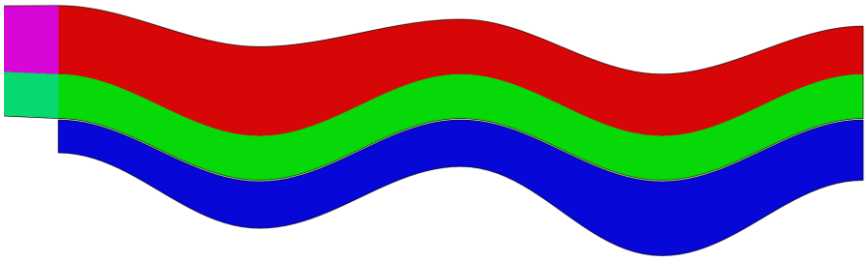

Fig. 8. Optimum design of fixture region in strut.

Table 4. Cross sectional dimensions of optimized design.

Dimension, in.	Station 4	Station 3	Station 2	Station 1	Station 0
Inner Radius (R_i)	1.250	0.975	1.200	0.875	1.150
Insert Thickness (t_i)	0.125	0.175	0.175	0.275	0.225
Overwrap Thickness (t_o)	0.250	0.325	0.200	0.225	0.175
Tube Thickness (t_t)	0.0936 (24 plies)				

Table 5. Balance of load in ramps.

Dimension, in.	Station 4	Station 3
Hoop strain (μ in./in.)	1432	1209
Ratio over average hoop strain (percent)	108.5%	91.5%

A 3D FE model of the MDU strut (model 2) was created from the geometry generated by the 2D axisymmetric model. This 3D model has two symmetry planes, at the midspan of the strut and another symmetry plane bisecting the strut into a 180° section, as shown in Fig. 9. The model consisted of 392,677 C3D8 continuum solid elements and 492,583 nodes. Two versions of this model were generated. In version 2a, the laminate properties were represented with smeared properties according to composite lamination theory (CLT), as was used with the 2D axisymmetric model. In version 2b, the actual laminate is represented by layered shells where it is acknowledged that the symmetry condition simulates an unrealistic herringbone effect.

An additional 3D model (model 3) was built with no symmetry planes as a fully comprehensive model of the MDU. Model 3 had 853,174 SC8R continuum shell elements and 1,062,520 nodes. Nonlinear static analyses were performed with all four models. Linear buckling analysis was performed only with Model 3; because, bending could not be simulated with the axisymmetric Model 1, and because the symmetric boundary conditions in Models 2a and 2b limited the number of mode shapes that could be simulated. For Model 3, the displacement (double the symmetric models) was applied to the metallic fixture at one end, while the displacements at the end of the other fixture were fixed.

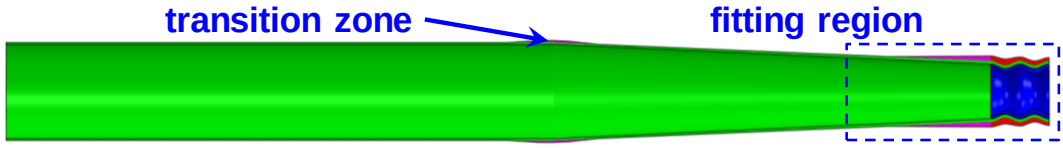

(a) Symmetric FE model of strut

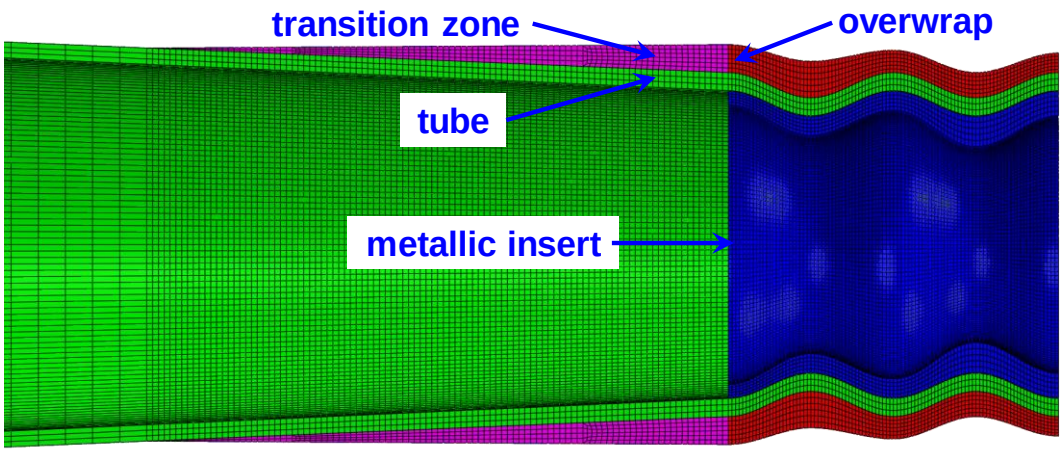

b) Detail of fixture region in FE model

Fig. 9. 3D finite element model of strut.

A load-displacement plot for the 2D and 3D models is presented in Fig. 10. The stiffnesses of the two symmetric 3D models were within 0.5% of the 2D model. The stiffness of the 3D model without symmetry was within 1.7% of the 2D model. Axial strain results in the middle of the strut for all four models are shown in Fig. 11. Strain results for the symmetric 3D models were within 0.1% of the 2D model. Strain results for the 3D model without symmetry were within 1.7% of the 2D model. The strains are essentially uniform in the straight tube section in the middle of the strut; so a color contour plot for the strains in the center of the strut was not presented.

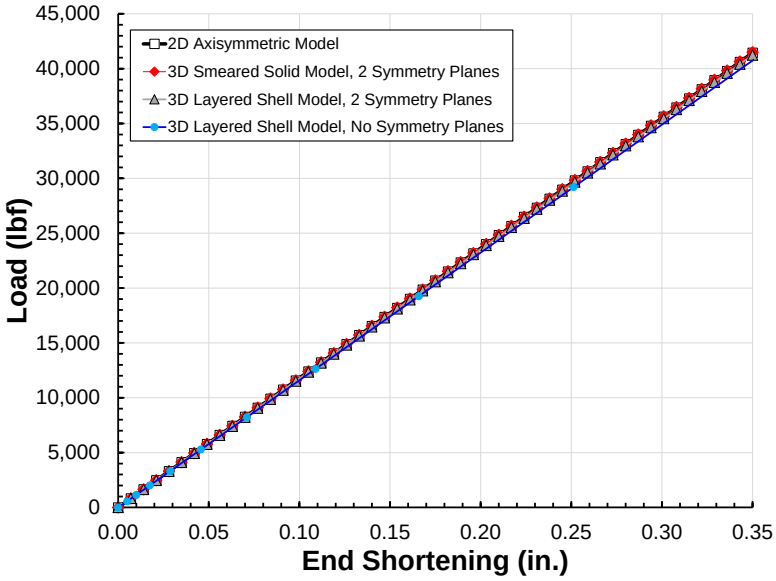

Fig. 10. Load-displacement plot.

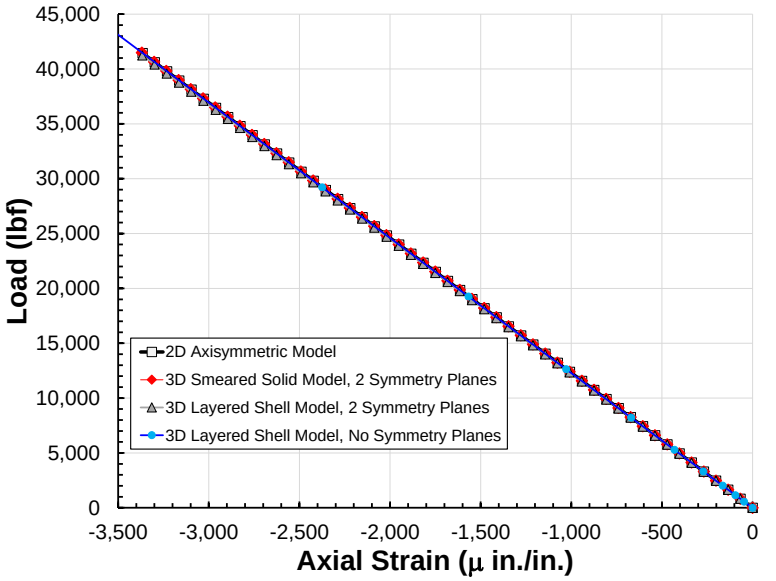

Fig. 11. Comparison of axial strain results in FE models of strut (far-field).

Coordinate systems for results display differed between the three models because of element formulation. The element result coordinate axes are described in Table 6. The axisymmetric elements in Model 1 required that the global 2-axis was the axis of revolution (as shown in Fig. 6a). A cylindrical coordinate system was used in all 3D models in which axes 1, 2, and 3 were radial, hoop, and axial, respectively. Stress and strain results in Model 2a are consistent with the cylindrical coordinate system. However, for the layered shell models, the laminate stacking direction is always the 3-direction, and the 1- and 2- axes are the axial and hoop directions, respectively. Element contour color results in Figures 12 to 14 correspond to the corresponding coordinate systems listed in Table 6.

Table 6. Element result coordinate systems.

Model	Axial Direction	Hoop Direction	Laminate Stacking Direction
Model 1, 2D Axisymmetric	Default 2 Global 2	Default 3 Global 3	Default 1 Global 1
Model 2a, 3D Symmetric Smeared	Default 2 Cylindrical 3	Default 3 Cylindrical 2	Default 1 Cylindrical 1
Model 2b, Symmetric Layered Shell	Cylindrical 1	Cylindrical 2	Cylindrical 3
Model 3, Full Layered Shell	Cylindrical 1	Cylindrical 2	Cylindrical 3

The von Mises stress results in the titanium fitting for the 2D axisymmetric and 3D models are shown in Fig. 12. Stresses are not shown in the composite tube or the overwraps. High stresses were found at station 0, station 2, and in the ramp between stations 2 and 3, as shown in Figs. 12b to 12d. Stresses in the two layered shell models were similar, so only the FE model for the symmetric layered shell model is shown. Maximum stresses for the smeared 3D model was within 2.1% of the stresses in the axisymmetric 2D model. Stresses in the region between stations 2 and 3 for the layered 3D model were within 0.5% of the stresses in the 2D model, but the stresses in this 3D model were higher at station 2.

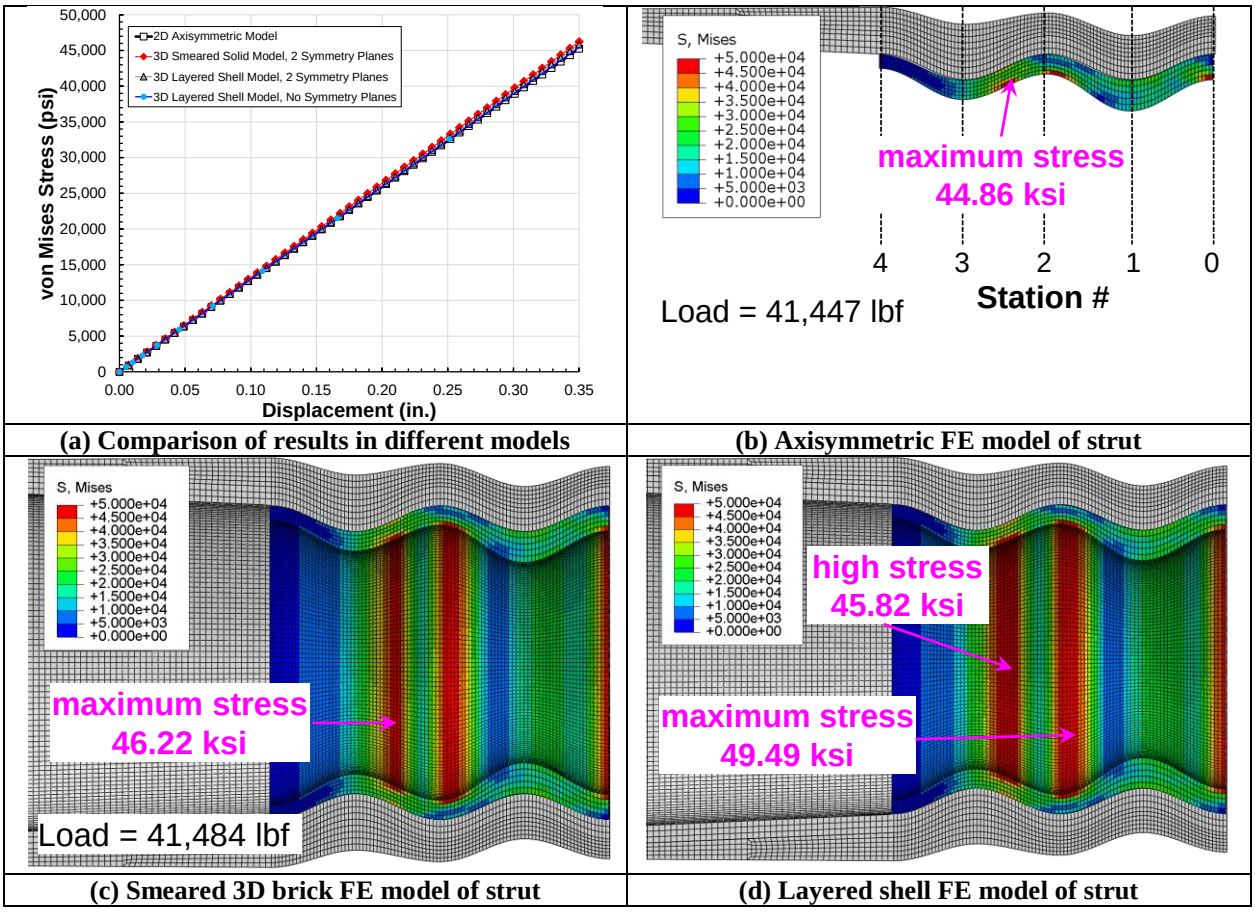

(a) Comparison of results in different models

(b) Axisymmetric FE model of strut

(c) Smeared 3D brick FE model of strut

(d) Layered shell FE model of strut

Fig. 12. Von Mises results in FE models of strut (fixture region).

Axial strain results in the fitting region for the 2D axisymmetric and 3D models are shown in Fig. 13. Strains are not shown in the metallic insert, which is shaded as light grey. High compressive strains were found at station 3, as shown in Figs. 13b to 13d. Strains in the overwrap were included in the 5000 microstrain constraint; so strains in the tube laminate were of greater interest. The minimum strain for the smeared 3D model was within 1.4% of the strains in the axisymmetric 2D model. The magnitudes of the minimum strain in the layered 3D models were 26% lower

than strains in the 2D model, but peak tensile and compressive strains occurred at similar locations in the layered shell and the smeared models. The difference in the strains is due to a combination of differences in the layered shell and smeared solid element representation of the composite properties and the nonlinear nature of the contact algorithm. Because the layered shell model is a more accurate representation of the actual stacking sequence, it is considered to be the more correct model. The axisymmetric model was preferred for the optimization study due to the ease of parameterization of the geometry and the much shorter analysis time (less than a minute) compared to the more accurate layered shell models (with analysis times of four to eight hours).

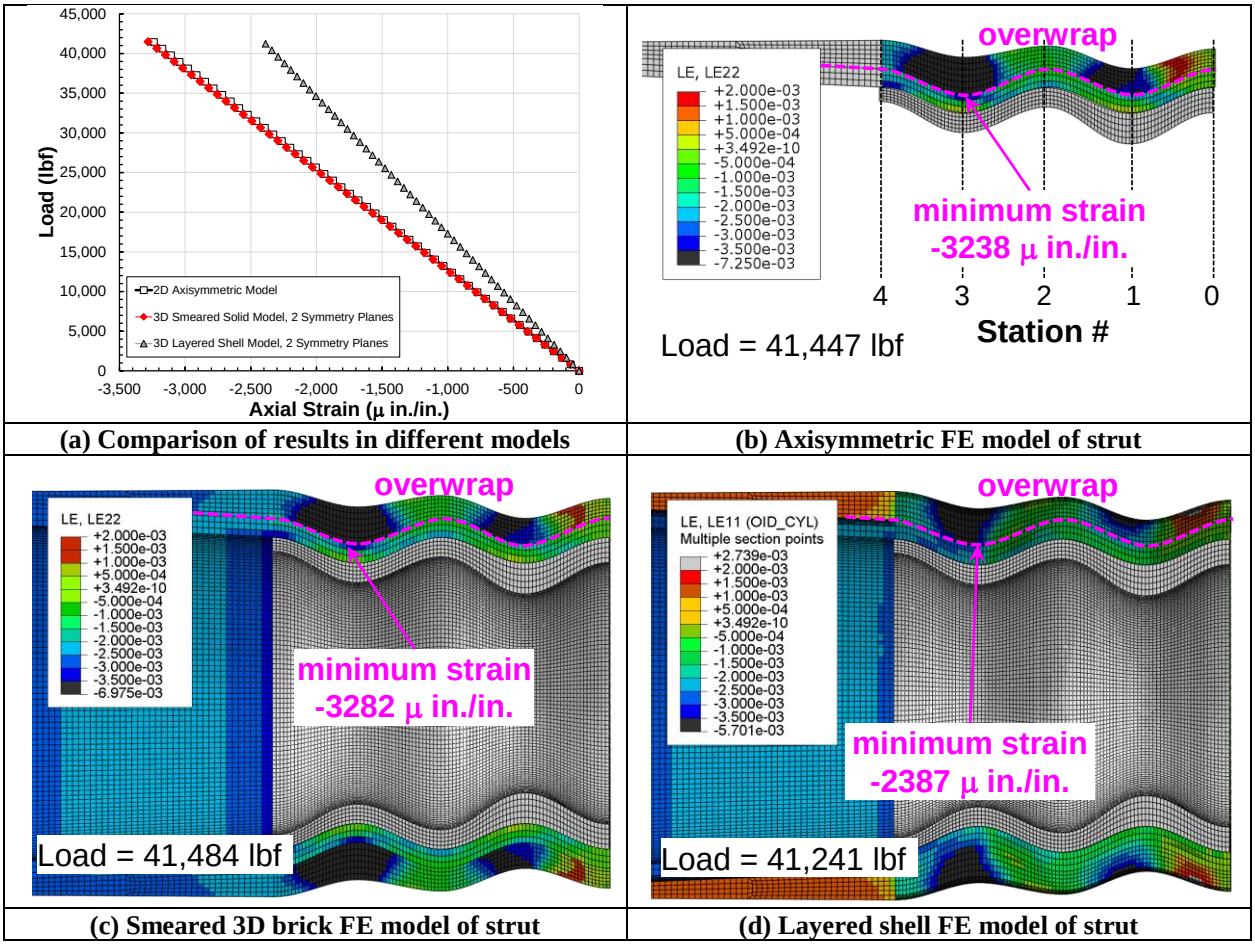

(a) Comparison of results in different models

(b) Axisymmetric FE model of strut

(c) Smeared 3D brick FE model of strut

(d) Layered shell FE model of strut

Fig. 13. Axial strain results in FE models of strut (overwrap in fixture region).

Hoop strain results in the fitting region for the 2D axisymmetric and 3D models are shown in Fig. 14. Strains are not shown in the metallic insert, which is shaded as light grey. High tensile strains were found in the ramp between station 0 and 1, as shown in Figs. 14b to 14d. The maximum strain for the smeared 3D model was within 1.8% of the strains in the axisymmetric 2D model. The maximum strain in the layered 3D models were 32% higher than strains in the 2D model, but peak tensile and compressive strains occurred at similar locations in the layered shell and the smeared models.

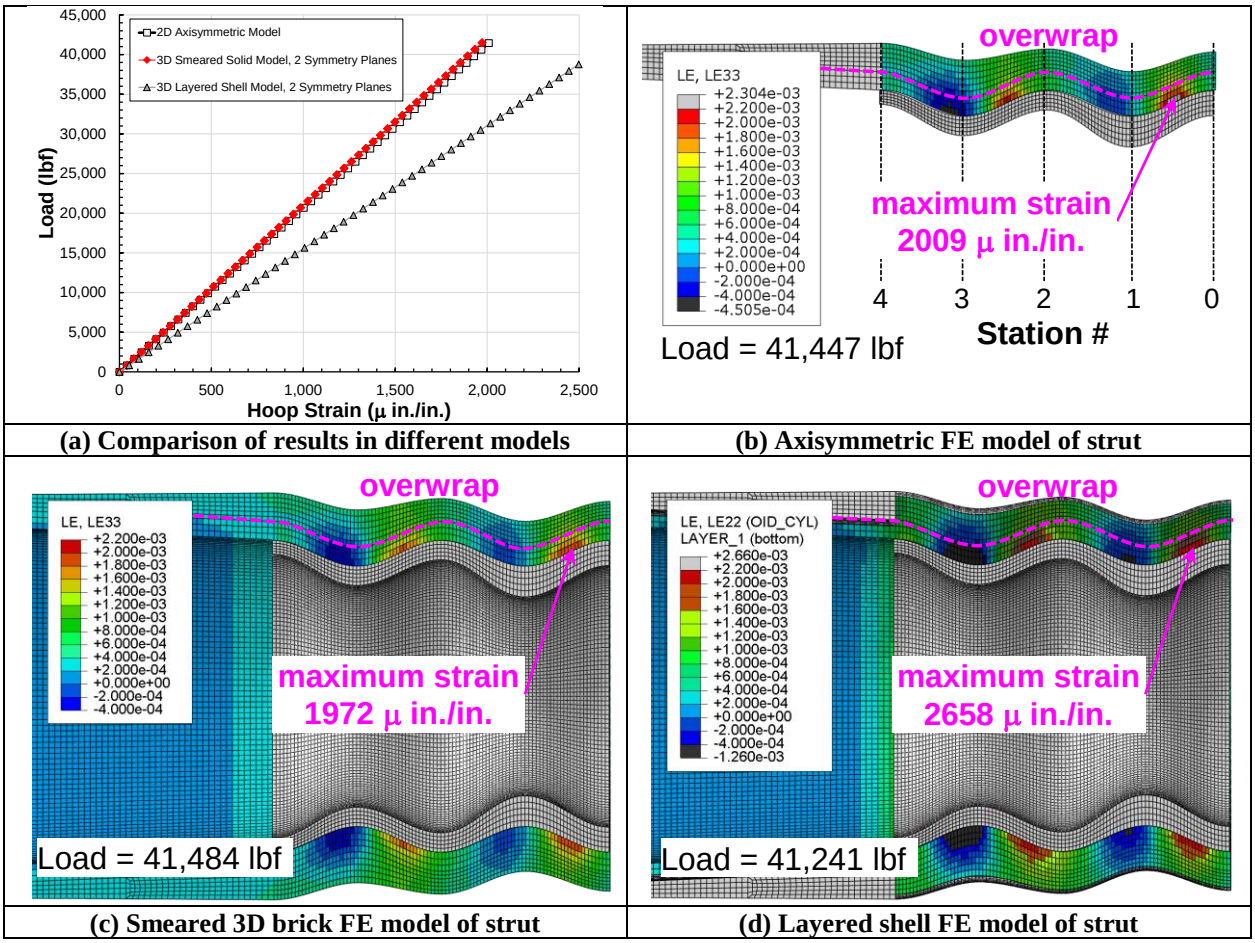

Fig. 14. Hoop strain results in FE models of strut (tube in fixture region).

The symmetric boundary conditions prohibited the use of buckling calculations in all models with symmetry, but buckling analyses were performed using the full 3D layered shell model. Buckling analysis was performed as a final step to validate the design and was not included in the optimization process. In the landing gear system, the boundary conditions at each end of the strut depend on the joint at each end (*e.g.* ball-and-socket, pin-and-clevis, and other types of joints).

In beams subjected to compression, clamped end conditions result in higher buckling loads than pinned end conditions. These two types of end conditions were used to bracket the range of buckling loads in the strut. Buckling loads for the strut range from 31.8 kips (for pinned end conditions) to 91.64 kips (for clamped end conditions), as shown in Figs. 15 to 17, respectively. Based on this buckling study, the current strut design (based on a 40.5 kip compressive load) is not suitable for a truss structure with two ball-and-socket joints (pinned end conditions), but the design is suitable for a truss structure with at least one clamped end.

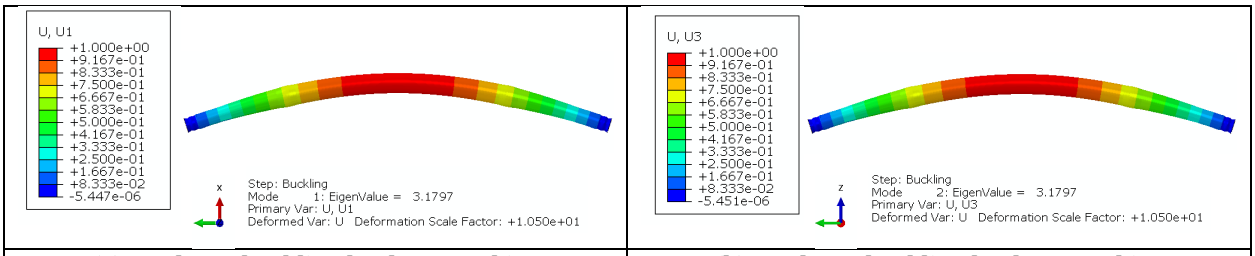

(a) Mode 1 – buckling load = 31.80 kips | **(b) Mode 2 – buckling load = 31.80 kips**

(c) Mode 1 – buckling load = 113.38 kips | **(d) Mode 2 – buckling load = 113.38 kips**

Fig. 15. Buckling results in FE models of the strut for the pinned-pinned end boundary condition

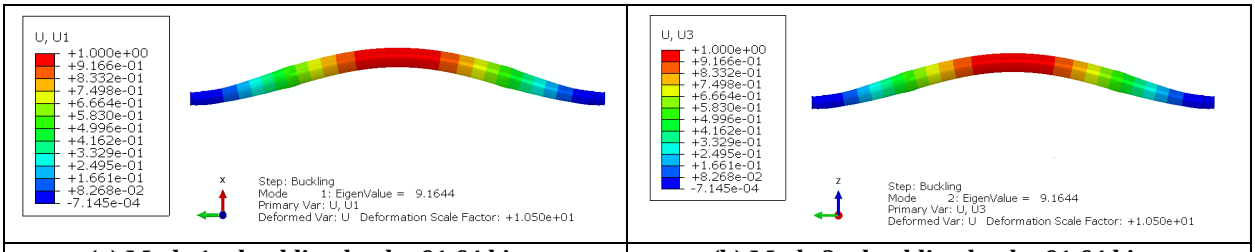

(a) Mode 1 – buckling load = 91.64 kips. | **(b) Mode 2 – buckling load = 91.64 kips.**

(c) Mode 3 – buckling load = 170.24 kips | **(d) Mode 4 – buckling load = 170.24 kips**

Fig. 16. Buckling results in FE models of the strut for the clamped-clamped end boundary condition.

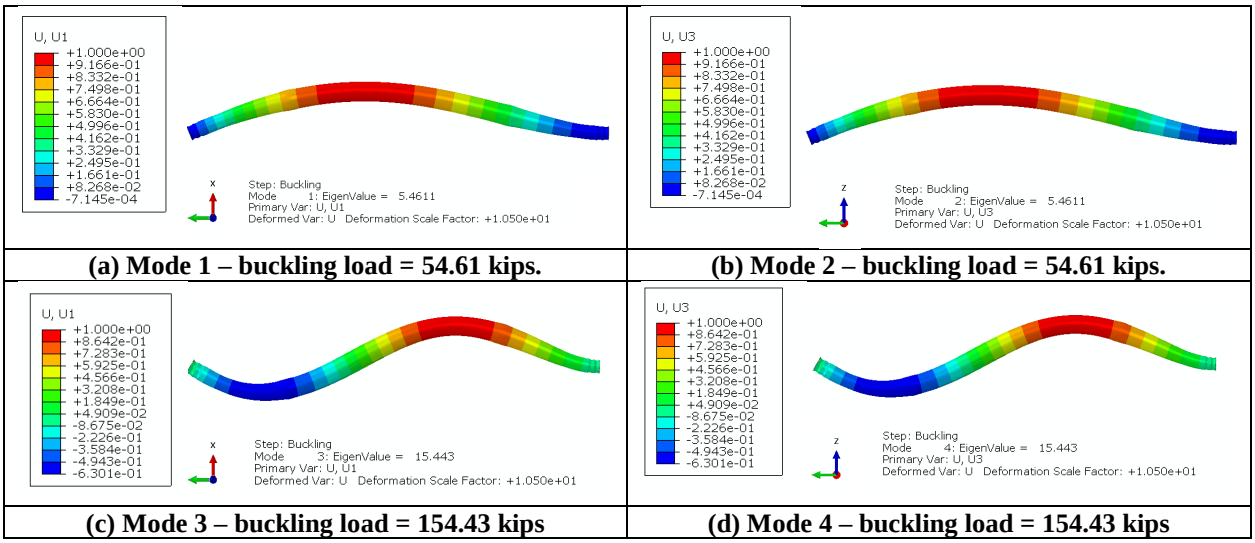

(a) Mode 1 – buckling load = 54.61 kips. | **(b) Mode 2 – buckling load = 54.61 kips.**

(c) Mode 3 – buckling load = 154.43 kips | **(d) Mode 4 – buckling load = 154.43 kips**

Fig. 17. Buckling results in FE models of the strut for the clamped-pinned end boundary condition.

VI. Concluding Remarks

In this paper, development of an optimization framework to design a landing gear strut was discussed. Baseline design parameters were developed from previous work by NASA and Northrop Grumman for the Altair landing gear struts. A tool for performing rapid optimization trade studies was also discussed. Results for 2D axisymmetric, 3D quarter-symmetric smeared property, 3D quarter-symmetric layered shell property, and full 3D finite element models were presented. Far-field strain and load-end shortening results for all 3D models were within 2.1% of the results for the 2D axisymmetric model. Similarly, all results for the 3D quarter-symmetry results were within 2.1% of the results for the 2D axisymmetric model. Localized strains in the fixture region of the 3D layered shell models were off by 20% to 30% from the smeared property models, but the peak strain patterns were similar. This mismatch in strains can be attributed to the difference in the element formulation and differences in property definition between layered shells and continuum solid elements. This mismatch could also have been due to the complicated nonlinear nature of the Abaqus contact algorithm in the vicinity of the strain values reported.

The models developed in this study will be used for development of a manufacturing design unit. The ISAAC facility will be used to manufacture this unit as a demonstration of the use of automated fiber placement to fabricate composite struts.

References

[1] Wagner, H., "Remarks on Airplane Struts and Girders under Compressive and Bending Stresses: Index Values," NACA TM 500, 1929.

[2] Dow, N. F., and Hickman, W. A., "Design Charts for Flat Compression Panels Having Longitudinal Extruded Y-Section Stiffeners and Comparison with Panels Having Formed Z-Section Stiffeners," NACA TN 1389, 1947.

[3] Williams, J., Anderson, M., Rhodes, M., Starnes, J., and Stroud, J., "Recent Developments in the Design, Testing and Impact-Damage Tolerance of Stiffened Composite Panels," NASA TM 80077, 1979.

[4] Williams, J. G., and Stein, M., "Buckling Behavior and Structural Efficiency of Open-Section Stiffened Composite Compression Panels," *AIAA Journal*, Vol. 14, No. 11, 1976, pp. 1618–1626.

[5] Williams, J. G., and Mikulas, M. M., Jr., "Analytical and Experimental Study of Structurally Efficient Composite Hat-Stiffened Panels Loaded in Axial Compression," *Proceedings of the 16nd AIAA/ASME/ASCE/AHS/ASC Structures, Structural Dynamics and Materials Conference*, Denver, CO, AIAA Paper 75-754, May 1975.

[6] Dow, N. F., and Rosen, B. W., "Structural Efficiency of Orthotropic Cylindrical Shells Subjected to Axial Compression," *AIAA Journal*, Vol. 4, No. 3, 1966, pp. 481–485.

[7] Haynie, W. T., and Hilburger, M., "Comparison of Methods to Predict Lower Bound Buckling Loads of Cylinders Under Axial Compression," *Proceedings of the 51st AIAA/ASME/ASCE/AHS/ASC Structures, Structural Dynamics and Materials Conference*, Orlando, FL; AIAA Paper 2010-2532, April 2010.

[8] Collins, T., and Nienaber, T., "Design and Analysis Cycle III Structures and Mechanisms Design Summary," Altair Structures and Mechanisms Subsystems, NASA, Presented at Johnson Space Center, Houston, TX, 25 June 2010.

[9] Brewster, J., "Design of Structurally Efficient Tapered Struts," NASA CR 2009-8393, Dec. 2009.
[10] Messinger, R., "Design of Structurally Efficient Tapered Struts," NASA CR 2010-216698, May 2010.
[11] Deo, R., Benner, H., Dawson, V., Olason, E., and Harrison, R., "Design of Structurally Efficient Tapered Struts (SETS)," NASA CR 2010-216699, May 2010.
[12] Messinger, R., "Design and Manufacturer of Structurally Efficient Composite Struts—Concept 1," Final Report for NASA Contract NAS NAS1-NNL04AA11B, Task NNL09AC35T, Nov. 2009.
[13] Pires, K., Benner, H., Deo, R., Grover, R., Palm, T., McLaughlin, M., Olason, E., Lucking, R., and Collier, C., "Design and Manufacturer of Structurally Efficient Composite Struts—Concept 2," Final Report for NASA Contract NAS NAS1-NNL04AA13B, Task NNL09AC36T, Jan. 2010.
[14] Wu, K. C., Phelps, J., McKenney, M., and Jegley, D., "Highly Loaded Composite Strut Test Development," *Proceedings of the 52nd AIAA/ASME/ASCE/AHS/ASC Structures, Structural Dynamics and Materials Conference*, Denver, CO, 2011; AIAA Paper 2011-1787.
[15] Jegley, D., Wu, K. C., Phelps, J., McKenney, M., Oremont, L., and Barnard, A., "Evaluation of Long Composite Struts," NASA TM-2011-217049, Feb. 2011.
[16] Jegley, D., Wu, K. C., Phelps, J., McKenney, M., and Oremont, L., "Structural Efficiency of Composite Struts for Aerospace Applications," *Proceedings of the 52nd AIAA/ASME/ASCE/AHS/ASC Structures, Structural Dynamics and Materials Conference*, Denver, CO, 2011; AIAA Paper 2011-1788.
[17] Jegley, D., and Wu, K. C., "Structural Efficiency of Composite Struts for Aerospace Applications," *Journal of Spacecraft and Rockets*, Vol. 49, No. 5, September-October 2012.
[18] T800S-3900 Data sheet, https://www.toraycma.com/.
[19] ABAQUS Version 6.12 EF1 Online Documentation, ABAQUS Analysis User's Manual, Dassault Systèmes Simulia Corp., Pawtucket, RI, 2012.
[20] Stander, N., Roux, W., Basudhar, A., Eggleston, T., Goel, T., and Craig, K., LS-OPT User's Manual: A Design Optimization and Probabilistic Analysis Tool for the Engineering Analyst, Livermore Software Technology Corporation, December 2015.
[21] McKay, M.D., Conover, W.J., Beckman, R.J. "A comparison of three methods for selecting values of input variables in the analysis of output from a computer code." *Technometrics*, Vol. 42, No. 1, pp. 239-245, 1979.
[22] Sacks, J., Schiller, S. B, and Welch, W. J.: "Design of Computer Experiments," *Technometrics*, Vol. 31, No. 1, February 1989.
[23] PATRAN 2016 Release Guide, MSC Software, MSC Software, Santa Ana, CA 92707.